Appl Phys B (2011) 105:509–515
DOI 10.1007/s00340-011-4582-4

Applied Physics B
Lasers and Optics

Nonlinear photoelectron emission from metal surfaces induced by short laser pulses: the effects of field enhancement by surface plasmons

S. Varró · N. Kroó

Received: 23 October 2010 / Revised version: 14 April 2011 / Published online: 4 June 2011

Abstract Nonlinear electron emission processes induced by surface plasmon oscillations have been studied both experimentally and theoretically. The measured above-threshold electron spectra extend up to high energies whose appearance cannot be explained solely by standard non-perturbative methods, which predict photon energy separated discrete energy line spectra with the known fast fall–plateau–cutoff envelope shape, even when taking the large field enhancement into account. The theoretical analysis of our data, based on the concept of plasmon-induced surface near-field effects, gives a reasonably good explanation and qualitative agreement in the whole intensity range.

1 Introduction

Surface plasmons (SPOs) are wave-like motions of conduction electrons on a metal surface, coupled with photons, e.g. the ones exciting these waves. The energy of these SPOs in this case is that of the exciting photons, but their wavelength is shorter. One of the main characteristics of the SPOs is their very large electromagnetic fields concentrated at the interfaces of metals and dielectrics (vacuum). To our knowledge, such an enhancement was first discussed by Fano [1] in 1938. Recently, this phenomenon has become the subject of extensive research, because on the basis of it high-order nonlinear processes can be induced even at relatively moderate intensities of incoming radiation which excites the SPOs [2–5]. In the case of a simple thick metal surface, the general theory predicts the well-known characteristic above-threshold 'fast fall–plateau–cutoff' envelope photoelectron shape, which consists of discrete spectral lines, repeated with steps of the exciting photon energy. It is, however, quite reasonable to expect that, due to the strongly nonlinear SPO-induced near-field effects, including the strong field enhancement, the photoelectron spectrum may have a different shape due to the mediating involvement of the resonantly excited SPOs on the thin metal film. Consequently, in addition to the perturbative–non-perturbative theories, valid for metals, the elaboration of our special theoretical model [6] seems to be feasible, which incorporates the special features of the SPO excitation process.

In our experiments, ∼80-fs Ti:Sa laser pulses (wavelength ∼800 nm, photon energy 1.5 eV) were used to excite SPOs at a thin gold surface in the Kretschmann geometry and the energy spectra of the generated photoelectrons have been analyzed by the time-of-flight technique. In these emission processes, a minimum of four times the plasmon energy is needed to overcome the work function (4.7 eV) and liberate the photo (plasmon) electrons. Relatively low laser intensities (in the range 2.70–23.1 $\times 10^8$ W/cm^2) have been used, and electrons of energies up to 40 eV were observed. The model of [6] is capable of explaining qualitatively these observations, too, and the analytic formula, derived from this model, has proven to be in a quite good (qualitative) agreement with the experimental data. Furthermore, according to our recent theoretical analysis [7], in line with these observations based on the huge SPO field enhancement, it cannot be excluded that the emitted electrons come out from the surface in attosecond pulse trains, due to the interference of the higher order above-threshold de Broglie waves at the metal surface, even in the case of the relatively moderate incoming laser intensities used.

S. Varró (✉) · N. Kroó
Research Institute for Solid State Physics and Optics, Hungarian Academy of Sciences, P.O. Box 49, 1525 Budapest, Hungary
e-mail: varro@mail.kfki.hu

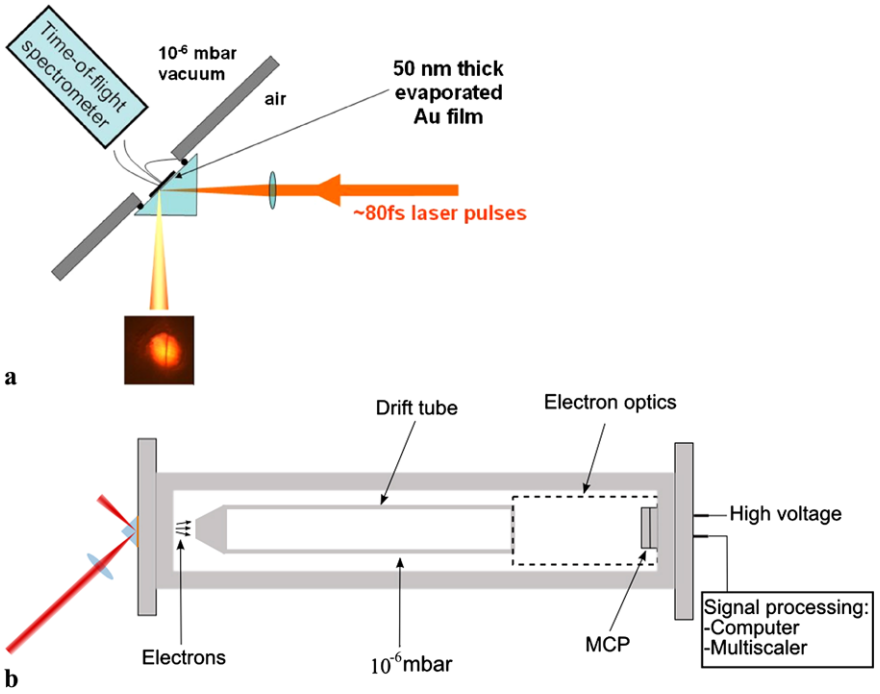

Fig. 1 Lay-out of the experiment (**a**) and of the time-of-flight spectrometer (**b**)

2 Experimental results

The aim of our experimental work has been to study and compare with theoretical predictions the spectral properties of SPO-emitted electrons at these moderate laser intensities. The lay-out of the experimental set-up is shown in Fig. 1a. The exciting light source was a frequency-doubled Nd:YAG laser pumped long-cavity Ti:Sa oscillator with a central wavelength of 800 nm and a pulse length of about 80 fs (after compression) with a repetition rate of 3.6 MHz. The average power of the light beam was about 600–700 mW. The laser pulses excited the SPOs in air via a glass prism in the Kretschmann geometry. The laser beam was focused on a 50-nm-thick gold film, deposited on the glass prism, by an 18.5 mm focal length lens (Fig. 1a). The SPO exciting laser intensity was changed by moving this lens out of focus. The emitted photoelectrons were analyzed in vacuum ($<10^{-6}$ Torr) by a time-of-flight spectrometer (Fig. 1b). The flight path of the electrons was 48.5 cm, the entrance aperture 0.7 cm and the acceptance angle 38°. In order to avoid frame overlapping of electrons coming from consecutive laser pulses at this high (3.6 MHz) repetition rate, a 5-eV positive drift voltage was applied. The detector was a multichannel plate multiplier (Photonic Chevron MCP) and its signals were recorded by a multichannel scaler with a time resolution of 100 ps. The slope of the photocurrent vs. laser intensity curve, when plotted in double-logarithmic scale, was linear at the lower end of the intensity with a slope of 4; at higher intensities the slope went down to around 2 and below.

Six typical electron spectra are shown in Fig. 2 for relatively low intensities. The number of electron pulses per laser pulse was far below 1, so no space-charge effects had to be considered. First, the laser intensity was varied in the ~59–200 MW/cm^2 range. For larger intensities the measured spectra become more structured, certainly because of possible heating effects or additional classical acceleration mechanisms. The count rate decreased significantly with increasing laser intensity. At the lower end of the laser intensity range the electron spectrum is peaked at around 5 eV and the detailed analysis of this spectrum shows some periodic structure in it, indicating the presence of above-threshold 4th, 5th, 6th etc. order currents induced by the SPO. At the upper end of the exciting laser intensity range the electron spectra are also peaked, but at maxima which are at higher energy and are shifted to higher electron energies with increasing laser intensity. The result of the Fourier transformation in these cases is a flat, structureless function. At intermediate laser intensities there is a continuous transition between the two cases presented in this figure. As seen in Fig. 2, we have not found plateaus in the electron spectra in the experiments which were carried out with relatively long laser pulses, comparable with the lifetime of the SPOs at this photon energy.

3 Theoretical considerations

In the prism of index of refraction $n = 1.5$ the incoming p-polarized laser radiation of circular frequency ω_0 is repre-

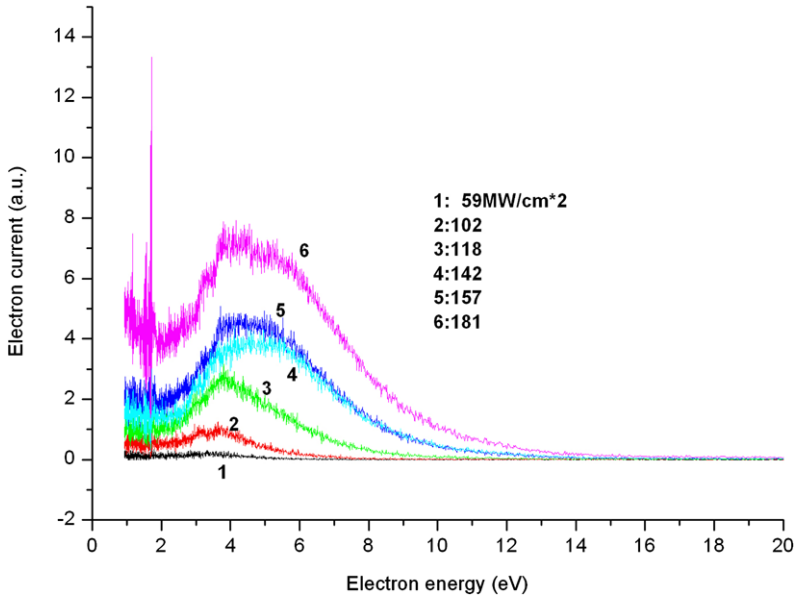

Fig. 2 Typical examples of the SPO-assisted electron spectra for relatively modest laser intensities (59, 102, 118, 142, 157 and 181 MW/cm^2). The curve labeled by '6' essentially corresponds to the theoretical plot (Fig. 3a) of the spectrum for the lowest intensity

sented by the electric field strength

$$\vec{E}_0 = (\vec{\varepsilon}_x \cos\theta_0 + \vec{\varepsilon}_z \sin\theta_0)|F_0| \times \cos\left[\omega_0\left(t - n\frac{x\sin\theta_0 - z\cos\theta_0}{c}\right) + \varphi_0\right], \quad (1)$$

where c is the velocity of light in vacuum, φ_0 is the phase of the complex amplitude F_0 and $\vec{\varepsilon}_x$ and $\vec{\varepsilon}_z$ are unit vectors being parallel and perpendicular to the metal surface, respectively. The numerical value $\varepsilon_2(\omega_0) = -\varepsilon_\mathrm{R} + \mathrm{i}\varepsilon_\mathrm{I} = -25.82 + \mathrm{i}1.63$ of the dielectric constant of the gold layer has been taken from Johnson and Christy [8]. With these parameter values, above the angle of total reflection $\theta_\mathrm{t} = 41.81°$, at the critical angle of incidence $\theta_0 = \theta_\mathrm{c} = 42.84° = \theta_\mathrm{t} + 1.03°$ the amplitude of the reflected wave drops practically to zero in a narrow angular range of half width of about 0.4°, and surface plasmon oscillations are generated at the metal–vacuum interface. In our experiments this 100% attenuated total reflection has been clearly observed. In our analytic calculations for the elliptically polarized electric field strength $\vec{E}_\mathrm{sp}$ representing the SPOs [9] in vacuum ($z > 0$), the following expression has been obtained:

$$\vec{E}_\mathrm{sp}(\vec{r}, t) = g|F_0|\mathrm{e}^{-x/2L_\mathrm{sp}}\mathrm{e}^{-z/2l_z}\left[\vec{\varepsilon}_z \cos(\omega_0 t' + \phi_0) - (\varepsilon_\mathrm{R} - 1)^{-1/2}\vec{\varepsilon}_x \sin(\omega_0 t' + \phi_0)\right], \quad (2a)$$

$$L_\mathrm{sp} \equiv \left|2\,\mathrm{Im}[k_\mathrm{sp}]\right|^{-1},$$
$$l_z = (\varepsilon_\mathrm{R} - 1)^{1/2}\lambda_0/4\pi, \quad (2b)$$
$$t' \approx t - (n_1 \sin\theta_\mathrm{c})(x/c).$$

In (2b), we have introduced the 'propagation length' $L_\mathrm{sp} \approx (\varepsilon_\mathrm{R} - 1)^2\lambda_0/2\pi\varepsilon_\mathrm{I}$ of the SPO, which is $\sim 61.6 \times \lambda_0 = 49\,\mu\mathrm{m}$ for $\varepsilon_\mathrm{R} = 25.82$, $\varepsilon_\mathrm{I} = 1.63$ and $\lambda_0 = c/\omega_0 = 795$ nm. The dimensionless factor g in the field amplitude in (2a) is about 12; thus, the direct SPO intensity enhancement is on the order of $g^2 \approx 150$ in the present case. If we take into account the geometrical field enhancement due to surface irregularities of spherical shape, then the maximum intensity enhancement factor was certainly about $\bar{g}^2 \approx 600$ in our experiments. It is seen in (2b) that in vacuum the SPO has an elliptically polarized electric field whose longitudinal x-component is smaller by a factor of $(\varepsilon_\mathrm{R} - 1)^{1/2} \approx 5$ than the z-component perpendicular to the metal surface. Inside the metal, on the other hand, the longitudinal component is larger by this same factor than the perpendicular one, so this latter is smaller by a factor of $(\varepsilon_\mathrm{R} - 1) \approx 25$ to compare with its value in vacuum. The fields inside the metal exponentially drop to their $1/\mathrm{e}$ values within the distance of $\lambda_0/31.3 \approx 25.4$ nm.

The Schrödinger equation of a metallic electron interacting with the SPOs reads

$$\hat{H}\psi(\vec{r}, t) = \mathrm{i}\hbar\frac{\partial\psi(\vec{r}, t)}{\partial t},$$
$$\hat{H} = \frac{1}{2m}\left(\hat{\vec{p}} + \frac{e}{c}\vec{A}_\mathrm{sp}\right)^2 + V, \quad (3)$$

where $\hat{\vec{p}} = -\mathrm{i}\hbar\nabla$ is the electron's momentum operator in coordinate representation, m is its mass and e is the elementary charge. The electric field strength $\vec{E}_\mathrm{sp}$ given by (2a) is connected with the vector potential $\vec{A}_\mathrm{sp}$ by the relation $\vec{E}_\mathrm{sp} = -\partial\vec{A}_\mathrm{sp}/\partial ct$. It is customary to use the Sommerfeld step potential model for the unperturbed electrons; thus, in the Hamiltonian given by (3), we take $V(z) = -V_0$ for $z < 0$ and $V(z) = 0$ for $z > 0$, where $V_0 = E_\mathrm{F} + W$ with

$E_F = 5.51$ eV and $W = 4.68$ eV being the Fermi energy and the work function, respectively, for gold. Besides, we are allowed to arbitrarily set $\varphi_0 = 0$ for the initial phase, because possible carrier–envelope phase difference effects [10, 18] are not relevant here, since in the experiments we have used relatively 'long' pulses containing more than 40 cycles. The electron transitions are induced at the metal–vacuum interface in a very narrow transverse spatial region, $|z| \ll \lambda_0$; thus, it is justified to use the usual dipole approximation. Moreover, it is well known [11] that the basic features of the surface photoelectric effect can be described by taking into account only the z-component of the electronic motion being perpendicular to the metal. This is because, at least according to the Sommerfeld model we are using, the electrons are moving freely along the metal surface, and in the photon (plasmon) absorption process only the z-component of the momentum changes significantly. In the dipole approximation and in one dimension, (3) simplifies to the equation

$$\begin{aligned} &\big[(\hat{p} + eA/c)^2/2m\big]\phi = \mathrm{i}\hbar\partial_t\phi, \\ &\hat{p} = -\mathrm{i}\hbar\partial/\partial z,\ \ A = (c/\omega_0)\bar{g}F_0\cos\omega_0 t, \end{aligned} \tag{4}$$

where now F_0 denotes the amplitude of the z-component of the electric field strength representing the incoming laser field and $\bar{g}^2 \approx 600$ is the total intensity enhancement factor, as has already been discussed above. The exact fundamental solutions of (4) are the non-relativistic version of the Volkov states which have long been widely used in strong-field physics [12]. They are modulated plane waves of the form

$$\begin{aligned} \phi_p(z,t) &= N\exp\big[(\mathrm{i}/\hbar)(pz - E_p t)\big] \\ &\quad\times \exp\big[-\mathrm{i}(\bar{g}\mu_0 pc/\hbar\omega_0)\sin\omega_0 t\big]\mathrm{e}^{-\mathrm{i}f(t)}, \\ E_p &= p^2/2m, \end{aligned} \tag{5a}$$

$$\begin{aligned} &\mu_0 \equiv eF_0/mc\omega_0 = 10^{-9}I^{1/2}\lambda_0, \\ &f(t) \equiv (1/\hbar)\int \mathrm{d}t\big(e^2/2mc^2\big)A(t). \end{aligned} \tag{5b}$$

In (5b), we have introduced the dimensionless intensity parameter μ_0 of the incoming laser radiation, whose numerical value can be easily calculated by the second equation in the defining equation, where the intensity I is measured in W/cm^2 and the wavelength λ_0 is measured in 10^{-4} cm. In the non-perturbative Keldysh-type description [11, 12], one would use the Volkov states, (5a), as final states and expand into a Fourier series the exponential with the sinusoidal modulation with the help of the Jacobi–Anger formula [13]

$$\begin{aligned} &\exp\big[-\mathrm{i}(\bar{g}\mu_0 p_n c/\hbar\omega_0)\sin\omega_0 t\big] \\ &\quad= \sum_{k=-\infty}^{\infty} J_k(\bar{g}\mu_0 p_n c/\hbar\omega_0)\mathrm{e}^{-(\mathrm{i}/\hbar)n\hbar\omega_0 t}, \\ &p_n = \sqrt{2m(-W + n\hbar\omega_0)}, \end{aligned} \tag{6}$$

where $J_n(x)$ are ordinary Bessel functions of first kind of order n. As a result, the n-plasmon absorption probability would be proportional to $J_n^2(\bar{g}\mu_0 p_n c/\hbar\omega_0)$. At the lowest intensity $I = 2\times 10^8$ W/cm^2 we used in our experiments $\mu_0 \approx 10^{-5}$ and, even if we take into account the enhancement factor $\bar{g} = 2\times 12$, the argument of the Bessel function would be on the order of or less than 1 and, of course, less than $n_0 = 4$, the minimum number of absorbed plasmons needed for the liberation of the electrons from the metal. In this case, owing to the asymptotic behavior of the Bessel functions $J_n^2(x) \approx [(x/2)^n/n!]^2$, the above-threshold peaks would exponentially drop, in sharp contrast to our experimental results. This means that on the basis of the standard non-perturbative description it is not possible to interpret the measured spectra, even if we take into account the considerable intensity enhancement of order 600, stemming from the SPO generation.

In order to have a satisfactory theoretical interpretation of our experimental results, as a next step in the analysis, we have applied the so-called 'laser-induced near-field' model which has long been introduced [14–16] by one of us (see also the more recent studies in [7, 9] and [6]). In this description, the basic interaction leading to very high nonlinearities is caused by the collective velocity field of the oscillating electrons near the metal surface, within a layer of thickness smaller that the penetration depth δ. Because the quasistatic velocity field is screened inside the metal, the thickness of the layer is taken as the Thomas–Fermi screening length $\delta_s = 1/k_{TF}$, where $k_{TF} = (6\pi n_e e^2/E_F)^{1/2}$. The concept of the laser-induced collective near field can be illustrated by the following physical picture. The electric field component of the radiation field being perpendicular to the surface makes the electrons oscillate, but the ionic cores remain stationary. According to Newton's second equation, these electrons acquire an additional oscillatory displacement $\vec{\alpha}(t) = \vec{e}_z\bar{g}\mu_0(\lambda_0/2\pi)\sin(\omega_0 t - \vec{k}_{||}\cdot\vec{x}_i)$ along the z-direction, which is superimposed to their average position $\vec{x}_i$. The additional potential energy of a test electron (the electron to be freed, with position $\vec{r}$) stems from the attraction of the ionic cores, and from the repulsion of the (now oscillating) electrons; $V_i(\vec{r}) = e^2/|\vec{x}_i + \vec{\alpha}(t) - \vec{r}| - e^2/|\vec{x}_i - \vec{r}|$, where the index i refers to the ith surface electron (which is associated on average to the ith ionic core). By summing up these contributions (in the continuum limit; $\sum_i V_i \to n_e\int \mathrm{d}^3x$), we obtain an oscillating double-layer potential acting on the test electron. Inside the metal the effect of this quasistatic field of the oscillating electron layer is only essential down to the Thomas–Fermi screening length δ_s; thus, the z-integration is restricted over this thickness. An inner test electron approaching the boundary periodically feels additional repulsion (negative excess charge) or attraction (positive excess charge), depending on the phase of the inducing electric field of the surface plasmon. Out of the metal ($z > 0$; in vacuum),

a similar situation occurs, but in an opposite manner, because there is an amplitude jump $V_D - (-V_D) = 2V_D$ in this potential on crossing the metal–vacuum boundary ($z = 0$). The wave function of an electron will then obey the two Schrödinger equations

$$\{[(\hat{p} + eA/c)^2/2m] - V_0 - V_D \sin\omega_0 t\}\Psi_I = i\hbar\partial_t \Psi_I \quad (z < 0), \tag{7a}$$

$$\{[(\hat{p} + eA/c)^2/2m] + V_D \sin\omega_0 t\}\Psi_{II} = i\hbar\partial_t \Psi_{II} \quad (z > 0), \tag{7b}$$

where the subscript I refers to the interior region (metal) and II to the exterior region (vacuum), respectively. Following Refs. [14–16], the amplitude of the collective velocity field is

$$V_D = 2\pi n_e e^2 \xi_0 \delta_s = \bar{g}\mu_0(\omega_p/4\omega_0)(\delta_s/\delta)\left(2mc^2\right), \quad V_D \approx \bar{g}\mu_0 \times 10^4 \text{ eV}, \tag{8}$$

where the dimensionless parameter μ_0 has already been defined in (5b) and δ denotes the skin depth of the metal at ω_0. Of course, the interaction with the SPO field in principle should still be taken into account, too, as in (4), but since its direct effect is much smaller than that of the induced collective velocity field, we have not displayed this direct interaction in (7a) and (7b). The time-averaged outgoing electron current components for which the momenta $p_n = [2m(n\hbar\omega_0 - W)]^{1/2}$ are real ($n \geq n_0 = 4$ in the present case), corresponding to nth-order multiplasmon absorption, have been obtained from the Fourier expansion of Ψ_I and Ψ_{II}. The unknown multiphoton reflection and transmission coefficients, R_n and T_n, respectively, can be determined from the matching equations, i.e. from the continuity of the wave function, $\Psi_I(0,t) = \Psi_{II}(0,t)$, and of its spatial derivative, $\partial_z\Psi_I(0,t) = \partial_z\Psi_{II}(0,t)$, which relations must hold for arbitrary instants of time. The resulting two coupled infinite sets of linear algebraic equations for R_n and T_n can be numerically solved without any particular difficulty; moreover, in our earlier works [14–16] we have derived quite accurate analytic approximate formulas, too. According to these results, the current components normalized to the incoming current can be expressed as

$$j_t(n) = (p_n/q_0)\cdot|T_n|^2, \quad |T_n|^2 \approx J_n^2(a) \quad (n \geq n_0),\ a \equiv 2V_D/\hbar\omega_0, \tag{9}$$

where $q_0 = (2mE_F)^{1/2}$ is the average of the initial momenta (see also Ref. [6]). For instance, in the case of $I = 2\times10^8$ W/cm^2 we have $2V_D \approx 11$ eV and $a = 2V_D/\hbar\omega \approx 7$, where we have taken for the ratio $\delta_s/\delta = 2\times10^{-2}$, i.e. for $\delta = 22.5$ nm the screening length is about $\delta_s \approx 0.4$ nm. This numerical example clearly shows that already at the lowest intensity used in the experiments the *new nonlinearity parameter a* introduced in (9) has a much larger value than the argument of the Bessel function in (6). On the basis of this remarkable quantitative difference, our theory based on introducing the laser-induced near field is capable of accounting for the basic features of the measured electron spectra. As we have seen before, in the frame of the standard *non-perturbative* Volkov description there is no chance to interpret this experiment, and several earlier experiments (as has also been emphasized in Refs. [7, 14–16], and [17]). The theoretical results are summarized in Fig. 3. The calculated above-threshold electron spectra are shown here for four different values of the incoming laser intensity, for illustrational purposes. We note that these figures have been generated without any adjustments, only on the basis of the formula in (9). Besides the numerical values of the natural constants c, $\hbar$, k, e and m, the experimental values of the optical constants of gold [8], its electron density $n_e = 5.9\times10^{22}/\text{cm}^3$ and the independently measured intensity of the laser have been used as input parameters for the calculation. Figure 3a corresponds to the experimental curve labeled by '6' in Fig. 2. A comparison with the experimental curves has shown that, in spite of the relative simplicity of our theoretical model based on the effect of the laser-induced near field at the metal–vacuum interface, the agreement is reasonable between experiment and theory. However, a qualitative discrepancy was found in higher laser intensity cases, where probably additional concurrent heating effects may have played some role. In the above model, these thermal and some other possible effects (e.g. due to resonant image potential states [19]) have not been taken into account.

In Fig. 4, we illustrate a comparison of the intensity dependence of the total current in the case of perturbation theory and according to our new non-perturbative description. For the side-bands of larger indices, the total current may be approximated by (if we neglect the n-dependence of the higher momenta) $j = \sum_n j_n \propto \sum_{n=5}^{\infty} J_n^2(a) = (1/2)[1 - J_0^2(a)] - [J_1^2(a) + J_2^2(a) + J_3^2(a) + J_4^2(a)]$, where the sum rule of the Bessel functions has been used; $\sum_{n=-\infty}^{\infty} J_n^2(a) = 1$. The $n = 4$ term is relatively small in comparison with higher terms, due to the smallness of the prefactor in $[(n\hbar\omega_0 - W)/E_F]^{1/2} J_n^2(\langle a\rangle)$ immediately close to threshold ($|4\hbar\omega_0 - W| \ll n\hbar\omega_0$). In the figure it is clearly seen that, though at even relatively low intensities there are quite many above-threshold electrons (as shown in Figs. 3a and 3b), the sum of the currents follows the 4th power perturbative law. For larger intensities, the 'degree of nonlinearity' $n(I) = \partial \log j/\partial \log I$ strongly deviates from $n = 4$, and the total current saturates, which is a naturally expected behavior.

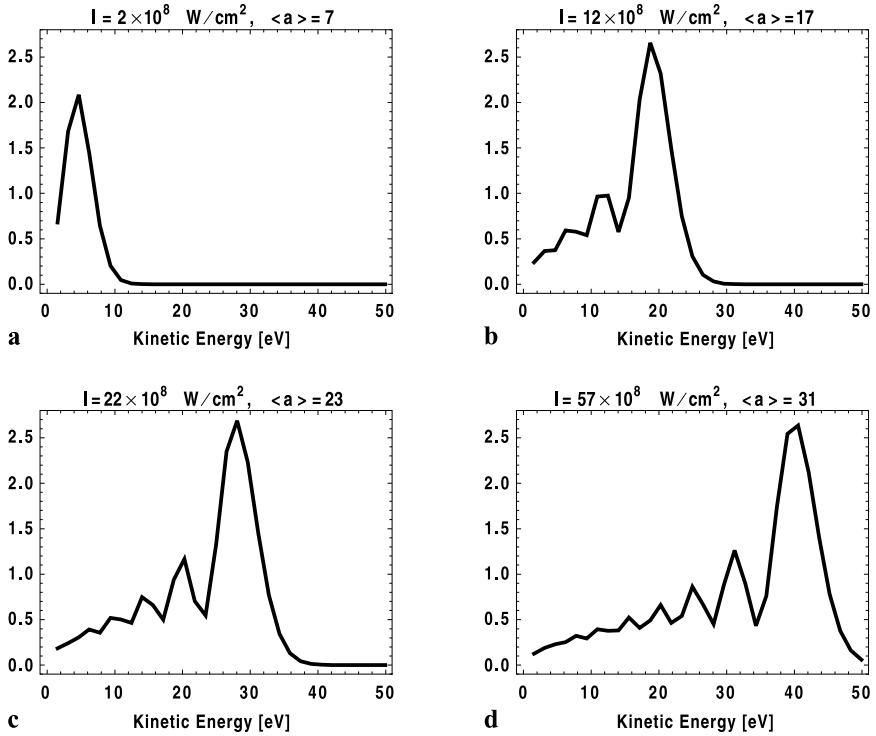

Fig. 3 The calculated above-threshold spectrum of the electron current ejected due to multiplasmon absorption. On the *vertical axes* we have plotted the normalized current, i.e. $10 \times [(n\hbar\omega_0 - W)/E_F]^{1/2} J_n^2(\langle a\rangle)$ for $n = n_0, n_0+1, \ldots, = 4, 5, 6, \ldots$, where $n_0 = 4$ is the minimum number of photons (plasmons) for the ejection. The values of the relative current components have been evaluated by taking the average of three neighboring values associated to the multiplasmon indices $n-1$, n and $n+1$. The *discrete points* are connected by *thick lines* in order to guide the eye. The parameter $\langle a\rangle = 2V_D/\hbar\omega_0$ is the ratio of the total jump of the plasmon-induced near-field potential at the metal–vacuum interface to the photon energy of the incoming laser radiation. The assumed intensities $I = \{2, 12, 22, 57\} \times 10^8$ W/cm^2 of the laser and the associated a-values $\langle a\rangle = \{7, 17, 23, 57\}$ are separately displayed in the plot labels of (**a**), (**b**), (**c**) and (**d**), respectively

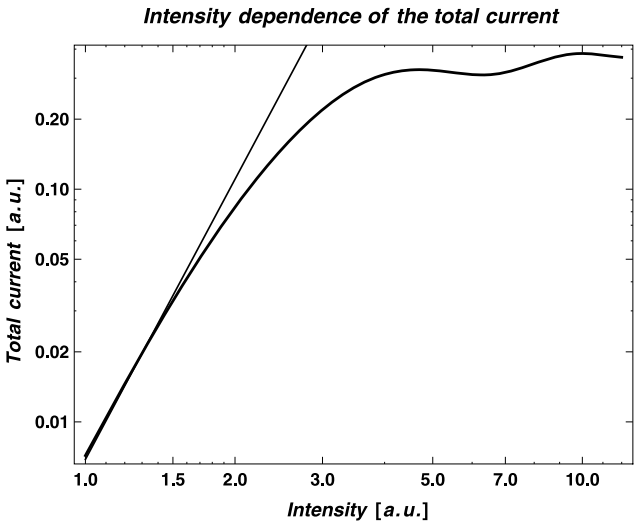

Fig. 4 The intensity dependence of the total photocurrent in a log–log plot, approximated only by the Bessel factors. The thin line represents the perturbative 4th power dependence $j \propto I^4$ (the function $f(x) = x^4/145$ has been drawn for comparison). The thick line shows the non-perturbative result, which has been approximated by $j \sim \sum_{n=5}^{\infty} J_n^2(a) = (1/2)[1 - J_0^2(a)] - [J_1^2(a) + J_2^2(a) + J_3^2(a) + J_4^2(a)]$, merely for illustrative purposes. Here $a = 7 \times \sqrt{x}$ has been taken, where the variable x is the dimensionless relative intensity (normalized to the smallest intensity value 2×10^8 W/cm^2)

4 Conclusions

A plateauless energy distribution of SPO-mediated electron emission was found when the pulse length of the SPO exciting laser was comparable with the lifetime of the surface plasmons. The electron emission was found to set in at relatively low laser intensities (10^8 W/cm^2) and the electron spectrum was found not to have a plateau, in contrast to expectations. In the Fourier transform of the energy spectra we have seen the discrete structure at low intensities, which comes out from our theory, too. On the other hand, the appearance of the large-energy electrons cannot be explained with standard non-perturbative theories, even if one takes into account the field enhancement due to the surface plasmons. If one takes some classical acceleration mechanism, one could perhaps explain the large-energy part of the spectrum, but, needless to say, one cannot account for the appearance of the discrete structure with spacing proportional to Planck's constant. The experimental results for lower laser intensities are reflected reasonably well in our theoretical calculations, in both the low-energy and the high-energy parts of the spectra. On the basis of these investigations, we conclude that both our experimental and the-

oretical results support the physical picture offered by our concept of a plasmon-induced oscillating near field (see [7, 14–16], and [17]) of a double layer at the metal–vacuum interface.

Acknowledgements This work has been supported by the Hungarian National Scientific Research Foundation OTKA, Grant No. K73728. The authors thank the referees for their valuable comments, which helped in improving the quality of the final version of the paper.

References

1. U. Fano, Ann. Phys. **32**, 393 (1938)
2. T. Tsang, T. Srinivasan-Rao, J. Fischer, Phys. Rev. B **43**, 8870 (1991)
3. M. Aeschlimann, C.A. Schmuttenmaer, H.E. Elsayed-Ali, R.J.D. Miller, J. Cao, D.A. Mantell, J. Chem. Phys. **102**, 8606 (1995)
4. S. Kim, J. Jin, Y.-J. Kim, I.-Y. Park, Y. Kim, S.-W. Kim, Nature **453**, 757 (2008)
5. J. Wu, H. Qi, H. Zeng, Phys. Rev. A **77**, 053412 (2008)
6. S. Varró, Gy. Farkas, Laser Part. Beams **26**, 9 (2008)
7. N. Kroó, S. Varró, Gy. Farkas, D. Oszetzky, A. Nagy, A. Czitrovszky, J. Mod. Opt. **54**, 2679 (2007)
8. P.B. Johnson, R.W. Christy, Phys. Rev. B **6**, 4370 (1972)
9. S. Varró, N. Kroó, Gy. Farkas, P. Dombi, J. Mod. Opt. **57**, 80 (2010)
10. S.E. Irvine, P. Dombi, Gy. Farkas, A.Y. Elezzabi, Phys. Rev. Lett. **97**, 146801 (2006)
11. G. Ferrini, F. Banfi, C. Gianetti, F. Parmigiani, Nucl. Instrum. Methods Phys. Res. A **601**, 123 (2009)
12. F.V. Bunkin, M.V. Fedorov, Sov. Phys. JETP **21**, 896 (1965)
13. A. Erdélyi (ed.), *Higher Transcendental Functions*, vol. II (McGraw-Hill, New York, 1953), Formula 7.2.4(26)
14. S. Varró, F. Ehlotzky, J. Phys. D, Appl. Phys. **30**, 3071 (1997)
15. S. Varró, F. Ehlotzky, Phys. Rev. A **57**, 663 (1998)
16. S. Varró, F. Ehlotzky, J. Phys. B, At. Mol. Opt. Phys. **31**, 2145 (1998)
17. N. Kroó, Gy. Farkas, P. Dombi, S. Varró, Opt. Express **16**, 21656 (2008)
18. F. Krausz, M. Ivanov, Rev. Mod. Phys. **81**, 163 (2009)
19. C. Kennerknecht, H. Hövel, M. Merschdorf, S. Voll, W. Pfeiffer, Appl. Phys. B **73**, 425 (2010)